


# Diagnostic Performance of a Lower-dose Contrast-Enhanced 4D Dynamic MR Angiography of the Lower Extremities at 3 T Using Multisegmental Time-Resolved Maximum Intensity Projections

Paul Raczeck, MD,\*  Peter Fries, MD, Alexander Massmann, MD, Peter Minko, MD, Felix Frenzel, MD, Tobias Woerner, MD, Arno Buecker, MD, and Guenther K. Schneider, MD

**Background:** For peripheral artery disease (PAD), MR angiography (MRA) is a well-established diagnostic modality providing morphologic and dynamic information comparable to digital subtraction angiography (DSA). However, relatively large amounts of contrast agents are necessary to achieve this.

**Purpose:** To evaluate the diagnostic accuracy of time-resolved 4D MR-angiography with interleaved stochastic trajectories (TWIST-MRA) by using maximum intensity projections (MIPs) of dynamic images acquired with reduced doses of contrast agent.

**Study Type:** Retrospective.

**Population:** Forty adult PAD patients yielding 1088 artery segments.

**Field Strength/Sequence:** A 3.0 T, time-resolved 4D MR-angiography with TWIST-MRA and MIP of dynamic images.

**Assessment:** DSA was available in 14 patients (256 artery segments) and used as reference standard. Three-segmental MIP reconstructions of TWIST-images after administration of 3 mL of gadolinium-based contrast agent (Gadoteridol/ Prohance<sup>®</sup>, 0.5 M) per anatomical level (pelvis, thighs, and lower legs) yielded 256 artery segments for correlation between MRA and DSA. Three independent observers rated image quality (scale: 1 [nondiagnostic] to 4 [excellent]) and the degree of venous overlay (scale: 0 [none] to 2 [significant]) for all segments. Diagnostic accuracy for the detection of >50% stenosis and artery occlusion was calculated for all observers.

**Statistical Tests:** Binary classification test (sensitivity, specificity, positive/negative predictive values, diagnostic accuracy). Intraclass correlation coefficients (ICCs), logistic regression analysis with comparison of areas under the receiver-operating-characteristics (ROC) curves (AUCs) with the DeLong method. Bland–Altman-comparison.

**Results:** High diagnostic performance was achieved for the detection of >50% stenosis (sensitivity 92.9% [84.3–99.9% (95%-CI)] and specificity 98.5% [95.7–99.8% (95%-CI)]) and artery occlusion (sensitivity 93.1% [77.2–99.2% (95%-CI)] and specificity 99.1% [96.9–99.9% (95%-CI)]). Inter-reader agreement was excellent with ICC values ranging from 0.95 to 1.0 for >50% artery stenosis and occlusion. Image quality was good to excellent for both readers ( $3.41 \pm 0.72$ ,  $3.33 \pm 0.65$ , and  $3.38 \pm 0.61$  [mean  $\pm$  SD]) with good correlation between observer ratings (ICC 0.71–0.81). No significant venous overlay was observed ( $0.06 \pm 0.24$ ,  $0.23 \pm 0.43$  and  $0.11 \pm 0.45$  [mean  $\pm$  SD]).

**Data Conclusion:** MIPs of dynamic TWIST-MRA offer a promising diagnostic alternative necessitating only reduced amounts (50%) of gadolinium-based contrast agents for the entire runoff vasculature.

**Evidence Level:** 3

**Technical Efficacy:** Stage 2

J. MAGN. RESON. IMAGING 2021;54:763–774.

View this article online at [wileyonlinelibrary.com](http://wileyonlinelibrary.com). DOI: 10.1002/jmri.27631

Received Jan 28, 2021, Accepted for publication Mar 23, 2021.

\*Address reprint requests to: P.R., Kirrberger Str. 1, 66421 Homburg/Saar, Germany. E-mail: paul.raczeck@uks.eu

From the Clinic for Diagnostic and Interventional Radiology, Saarland University Medical Center, Homburg, Saarland, Germany

This is an open access article under the terms of the Creative Commons Attribution-NonCommercial-NoDerivs License, which permits use and distribution in any medium, provided the original work is properly cited, the use is non-commercial and no modifications or adaptations are made.

Peripheral artery disease (PAD) is a severe manifestation of primarily atherosclerotic artery disease with significant clinical morbidity and mortality due to cardiovascular associated deaths.<sup>1,2</sup>

Digital subtraction angiography (DSA) is widely regarded as the diagnostic reference standard primarily because dynamic flow information is reliably obtained.<sup>3</sup>

However, its invasiveness and cost, as well as its requirement for ionizing radiation, have led to the development of MR-angiography (MRA) as an alternative, either as a multistation contrast-enhanced (ce) MRA or as a time-resolved (TR) MRA. MRA has high diagnostic accuracy and is often considered as the imaging modality of choice.<sup>4-6</sup>

Computed tomography angiography (CTA) is still regarded as the quickest and most widespread imaging tool available for evaluation of PAD, but its compromised diagnostic efficacy due to atherosclerotic calcifications in small vessels and the lack of dynamic flow information are well-known limitations.<sup>7</sup>

Evaluation of PAD with nonenhanced MRA techniques, such as quiescent interval single-shot (QISS) MRA unfortunately do not yield dynamic flow information and are prone to venous overlay, especially in atherosclerotic small vessels at the lower extremities.<sup>8-10</sup> Dynamic flow analysis is particularly important to assess the hemodynamic relevance of stenoses, especially in smaller vessels, and unfortunately motion artifacts, venous overlay and partial volume effects often substantially limit diagnostic accuracy.<sup>11</sup>

Therefore, “hybrid MRA” that combines multistation ce-MRA with TR-MRA has been established as the MRA modality of choice. This has high diagnostic efficacy and accuracy comparable to DSA and minimizes diagnostic pitfalls such as venous overlay.<sup>12-15</sup> However, dynamic flow information with this approach is only acquired for the infrapopliteal vessels and depending on inflow and collateralization, venous overlay in ce-MRA can often occur.

A possible approach to solving this problem is “triple-TWIST” MRA.<sup>16</sup> This technique consists of a triple injection protocol for dynamic, high resolution, isotropic MRA of the entire peripheral vascular system applying time-resolved 4D TWIST-MRA sequences (time-resolved angiography with interleaved stochastic trajectories). Thus, flow of the pelvic, thigh, and infrapopliteal artery stations can be separately analyzed yielding dynamic information of reduced or even reversed flow in each anatomic region.<sup>16</sup> However, in a clinical study that adopted this technique at 1.5 T, relatively large amounts of the gadolinium-based contrast agent (GBCA) gadobutrol (Gadovist®; Bayer Healthcare, Germany) were used 1 M concentration, 15 mL total volume applied, corresponding to 30 mL of a standard 0.5 M GBCA. The authors acknowledged that a higher accumulative dose was used than would ordinarily be needed for conventional ce-MRA with gadobutrol necessitates.

Since controversy still surrounds the intracerebral retention of Gd following GBCA administration, and with emerging

evidence that Gd is retained to a certain extent in specific brain areas after administration of all available GBCAs, new low-dose approaches to MR imaging are desirable.<sup>17,18</sup>

MRA at higher magnetic field strengths such as 3 T yields higher signal-to-noise ratio (SNR), thereby allowing shortening of the acquisition time and improvement of spatial resolution compared to that achievable at lower field strengths.<sup>19</sup> Furthermore, the longer T1 relaxation times of stationary background tissue at 3 T improve background tissue suppression which further enhances contrast-to-noise.<sup>20</sup> Consequently, higher field strengths allow the amount of GBCA to be reduced without substantial detriment to image quality.<sup>21</sup>

An additional practical problem of dynamic 4D MRA sequences is the large amount of image data acquired. Reading of all original image slices is laborious and time-consuming.

The purpose of this study was to evaluate the diagnostic performance of a new low-dose approach in triple-TWIST MRA at 3 T in patients with known or suspected PAD. Initially, to minimize reading time, only maximum intensity projections (MIPs) of the source images were evaluated with additional images evaluated only if warranted in cases of questionable pathologic findings.

## Materials and Methods

### Study Population

This retrospective study had institutional review board approval for the image evaluation. Written clinical and research informed consent was acquired for DSA and MRA from all patients.

From October 2017 to February 2019, 40 patients with known PAD or symptoms of PAD underwent triple-TWIST MRA and were included in this study.

Patient demographics are presented in Table 1.

Patient inclusion criteria were referral for suspected PAD and feasibility of evaluation by MRA. Feasibility comprised immediate availability of the MR scanner at our institution (7 AM to 22 PM, Monday to Friday) and general patient compliance in terms of limb pain attributed to possibly symptomatic PAD.

Exclusion criteria were common contraindications for MRA such as pacemakers, cochlea ear implants, claustrophobia, pregnancy as well as severe allergic predisposition to GBCA. Since this study used a low-dose approach (9 mL total volume, corresponding to ~0.05 mmol/kg bodyweight in a 75 kg weighing patient), severely impaired kidney function was not an exclusion criterion.<sup>22</sup>

Selective DSA was performed in 16 of these patients either as a therapeutic interventional procedure or when MR angiograms suggested pathologic conditions that warranted further investigation (Fig. 1). Patients were referred for selective DSA no later than 5 days after the MRA examination.

### MR Imaging Protocol

Imaging was performed on a 3.0 T system (Magnetom VIDA®; Siemens Healthineers, Erlangen, Germany, gradient strength 60 mT/m, slew rate 200 T/m/s). One flexible 18-channel phased-array radiofrequency (RF) long body coil and a dedicated 36-channel peripheral vasculature RF coil as well as a 32-channel RF spine array coil were used for data

**TABLE 1. Patient demographics**

Patient characteristics ( <i>n</i> = 40)	
Mean age in years (range)	64.36 (15–94)
Gender	
Male	22 (55%)
Female	18 (45%)
Metal hip prosthesis	4 (10%)
Lower limb amputation	6 (15%)
AV-fistula	3 (7.5%)
Aortic stents	2 (5%)
Iliac artery stents	5 (12.5%)
Femoral artery stents	7 (17.5%)
Femoral popliteal bypass graft	2 (5%)
Mid aortic syndrome	1 (2.5%)
Entrapment of popliteal artery	1 (2.5%)

Numbers are either mean with range in parenthesis or total numbers with % in parenthesis.

acquisition. All patients were placed in the supine position, feet first. An 18G i.v. access was placed in the left or right cubital vein.

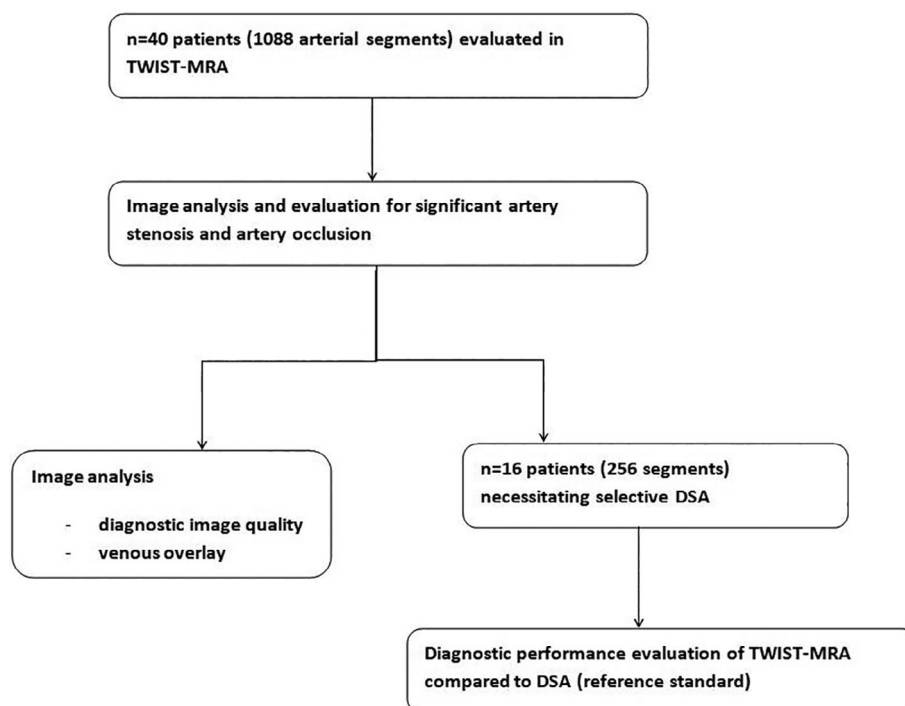
Three anatomic levels (pelvis, thighs, and lower legs) were covered by acquisition of coronal 3D datasets after automatic contrast injection, with slight overlap of the corresponding volumes.

Automatic injection (Accutron MR3, Medtron AG, Saarbruecken, Germany) of GBCA was performed. A 3 mL volume of gadoteridol (ProHance<sup>®</sup>, 0.5 M; Bracco Imaging, Milano, Italy) was administered at 2.5 mL/sec for each anatomic level, followed by a 25 mL saline flush also at 2.5 mL/sec. Thus, a total cumulative volume of 9 mL (3 × 3mL) gadoteridol was administered per patient.

A modified time-resolved MRA sequence (TWIST; Siemens Healthineers, Erlangen, Germany) was used for each anatomic area (Table 2). This imaging sequence applies partial *k*-space undersampling, with emphasis on more frequent sampling of the center of *k*-space compared to the periphery of *k*-space (“key hole” imaging). Missing data points in the peripheral *k*-space for each sequential dataset are obtained from adjacent *k*-space intervals (“view sharing”).<sup>23</sup>

In our modified protocol, sampling density was 15% for the central *k*-space and 20% for the peripheral *k*-space, with variation of peripheral *k*-space sampling trajectories throughout each sequential measurement.<sup>24</sup> Parallel acquisition (GRAPPA, acceleration factor 3 or 4) was applied and spatial resolution and coverage were adapted for each station (see Table 2). By combining parallel acquisition with TWIST-MRA, the resulting full 3D dataset was acquired with a temporal resolution of 4.5 seconds. Acquisition of up to 20 sequential 3D datasets covered a time span of sequential measurements with a temporal footprint of 12.7 seconds in the lower leg region. For the pelvis and thigh regions, the temporal resolution per single 3D dataset was 2.32 seconds with a total of up to 16 sequential measurements yielding a temporal footprint of 7.3 seconds.

Image acquisition was started 4 seconds–6 seconds before contrast administration. This ensured, that at least one unenhanced, precontrast 3D dataset was obtained for each anatomic level, allowing for image subtraction using an unenhanced initial 3D dataset as subtraction mask. Subsequently, dynamic subtracted 3D MIPs in coronal orientation were created demonstrating the inflow of

**FIGURE 1: Flow chart of evaluation procedure**

**TABLE 2. Image Parameters of TWIST-MR Angiography for Three Anatomic Stations**

	Pelvis	Thigh	Lower legs
Voxel size (mm <sup>3</sup> )	1.3 × 1.3 × 2	1.3 × 1.3 × 2	1.3 × 1.3 × 1
Slices	56	56	64
3D block partial Fourier factor	6/8	6/8	6/8
TR (msec)	2.66	2.66	2.62
TE (msec)	0.92	0.92	0.95
Flip angle	17°	17°	25°
Temp. resolution (seconds)	2.32	2.32	4.5
Temporal footprint (seconds)	7.26	7.26	12.7
Acquisition time (min:sec)	1:03	1:03	1:56
FOV (mm <sup>2</sup> )	500 × 437.5	500 × 437.5	500 × 437.5
GRAPPA imaging factor	4	4	3
Bandwidth (Hertz per pixel)	650	650	650

FOV = field of view; GRAPPA = generalized autocalibrating partially parallel acquisition.

contrast in the vessel territory of each anatomic level. Finally, static 3D MIP with maximum projection reconstructions (MPR) (72 views, 5° steps of angulation) fusing all three anatomic levels were generated to depict the entire runoff vasculature.

### Digital Subtraction Angiography Protocol

Selective DSA was performed in 16 patients no later than 5 days after the MRA study. Two experienced interventional radiologists (A.M and P.M., with 15 years and 12 years of experience in interventional radiology, respectively) performed intra-arterial DSA as the chosen reference standard (Artis Zee; Siemens Healthineers, Erlangen, Germany). A common femoral artery approach was used with a contralateral femoral retrograde access. A 4F Pigtail-catheter was positioned either approximately 2 cm proximal to the bifurcation of the infrarenal aorta or 2 cm proximal to the femoral bifurcation. Angiograms of the symptomatic region in posterior–anterior and angulated projections were obtained using 5 mL–10 mL of non-ionic iodinated contrast medium (300 mg of iodine per milliliter; Imeron 300, Bracco Imaging, Milano, Italy) per single DSA (4 frames/sec in the pelvic region, 2 frames/sec in the upper leg region, and 1 frame/sec in the lower leg region). The total amount of iodine contrast agents administered ranged from 25 mL to – 75 mL per patient depending on the number of DSAs necessary.

### Image Analysis

MR image data sets were displayed as dynamic, subtracted 3D MIP images in random order, with all acquired sections provided. For image analysis, the anatomic regions of arteries beginning at the aorta just below the level of the renal arteries to the calves were divided into 27 segments (Table 3). Three independent radiologists (P.F., P.R. and T.W.; with 15, 6, and 5 years of experience in vascular imaging, respectively) independently evaluated all MRA images

using a dedicated PACS workstation (SECTRA IDS 7 workstation, Sectra AB, Linköping, Sweden).

Initially, dynamic coronal MIP images were reviewed. Only if questionable pathologic findings were seen, additional 3D MPR images were analyzed. For imaging findings, deemed nondiagnostic or inconclusive, the original source images were also made available for review.

Reviewers rated overall image quality and arterial segment depiction based on a 4-point Likert-Score (4, excellent image quality, with enhancement allowing highly confident diagnosis; 3, good image quality, with adequate enhancement for diagnosis; 2, fair image quality, but still diagnostic; and 1, poor image quality, with blurring of the arterial segment and nondiagnostic).<sup>25,26</sup>

In addition, venous contamination was rated using a three-point scale (0, absence of venous overlay; 1, slight to moderate venous overlay not compromising diagnostic confidence; and 2, substantial venous overlay impairing diagnostic confidence).

The grading system for severity of artery stenosis was adopted from that used by the American College of Radiology for a multicenter evaluation of MRA.<sup>27</sup>

The three readers reviewed the dynamic subtracted 3D MIP images on a segment-by-segment basis and evaluated each arterial segment in terms of hemodynamically relevant (>50%) artery stenosis or artery occlusion.

Minimal diameter stenosis (DS) values were measured by each reader in the pelvic and thigh region.

### Statistical Analysis

The findings from DSA and TR-MRA sequences were compared on a segment by segment basis.

Positive and negative predictive values, sensitivity, specificity, and overall diagnostic accuracy were calculated for the detection of

**TABLE 3. Artery Segments Used for Image Analysis**

Segment number with corresponding anatomic vascular segment

- 1 Infrarenal aorta
- 2 Right common iliac artery
- 3 Left common iliac artery
- 4 Right external iliac artery
- 5 Left external iliac artery
- 6 Right common femoral artery
- 7 Left common femoral artery
- 8 Right proximal superficial femoral artery
- 9 Left proximal superficial femoral artery
- 10 Right distal superficial femoral artery
- 11 Left distal superficial femoral artery
- 12 Right popliteal artery
- 13 Left popliteal artery
- 14 Right tibiofibular tract
- 15 Left tibiofibular tract
- 16 Right proximal anterior tibial artery
- 17 Left proximal anterior tibial artery
- 18 Right distal anterior tibial artery
- 19 Left distal anterior tibial artery
- 20 Right proximal posterior tibial artery
- 21 Left proximal posterior tibial artery
- 22 Right distal posterior tibial artery
- 23 Left distal posterior tibial artery
- 24 Right proximal fibular artery
- 25 Left proximal fibular artery
- 26 Right distal fibular artery
- 27 Left distal fibular artery

major (>50%) artery stenosis as well as artery occlusions using the corresponding DSA images as reference standard. Corresponding 95% confidence intervals were provided for each diagnostic performance evaluation. Areas under the receiver-operating-characteristic (ROC) curves (AUC) were calculated for DS. Comparison of AUCs was performed with the help of the DeLong test.

Inter-reader agreement of contingency analysis was determined with the intraclass correlation coefficient (ICC) to determine inter-rater reliability (two-way, mixed model, absolute agreement). ICC values less than 0.5 are indicative of poor reliability, values between 0.5 and 0.75 indicate moderate reliability, values between 0.75 and 0.9 indicate good reliability, and values greater than 0.90 indicate excellent reliability.

Image quality and venous overlay scores were summarized by calculating means and standard deviations for each reader. Intraclass correlation coefficients (ICCs) were calculated to assess correlation of ratings between readers. Probability of true correlation in order to reject the null hypothesis was evaluated by calculating *P*-values for each correlation.

*One-way analysis of variances* (ANOVAs) with Bonferroni–Holm correction was also performed to compare ratings between readers.

A *P*-value < 0.05 indicated statistical significance.

All statistical analyses were performed using commercially available software (Prism<sup>®</sup> 7 for Windows, Version 7.00, GraphPad Software Inc., San Diego, CA, USA and MedCalc Software Ltd., Version 19.6.4, Ostend, Belgium).

## Results

Each reader evaluated 1088 segments across the 40 patients that underwent MRA. All arterial segments were judged to be sufficiently diagnostic (all image quality scores > 1).

Vessel segments with arterial stents, adjacent hip or knee prostheses were poorly visualized because of susceptibility artifacts.

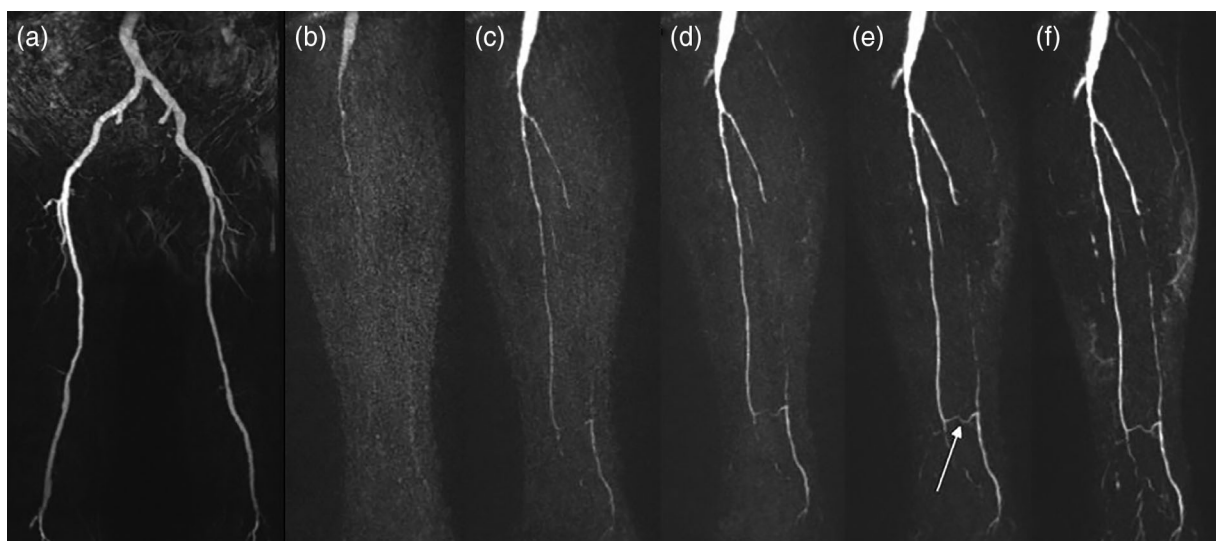


**FIGURE 2:** 85 year-old-male patient with known PAD. (a) MIP/MPR of subtracted TWIST images of entire lower extremities reveal multiple significant artery stenoses and occlusions on both lower legs, with a severe stenosis of the right posterior tibial artery (arrow) accompanied by intact perfusion of the distal vessel segments. (b–f) Dynamic image analysis of the right lower leg however reveal a total occlusion of the right posterior tibial artery, with retrograde perfusion by a distally located small collateral artery between the right distal fibular artery and the right distal posterior tibial artery (arrow). This finding could only be concluded due to available dynamic flow information.

However, dynamic flow comparison of both ipsi- and contra-lateral adjacent arterial vessel segments yielded sufficient information for determination of significant (in-stent) artery stenosis or occlusions. Clinical examples are provided in Figs. 2 and 3.

### Diagnostic Performance

MRA and DSA were available in 256 arterial segments in 16 patients.

In total, 62 significant artery stenoses (11 in pelvic segments, 23 in thigh segments, and 28 in lower leg segments) and 27 artery occlusions (1 in pelvic segments, 7 in thigh segments, and 19 in lower leg segments) were diagnosed at DSA. Of these, 96.5%–100% (depending on location and reader) were successfully detected at MRA.

The performance of the three readers for the detection of hemodynamically relevant *stenosis* and occlusion is presented in Tables 4 and 5, respectively.

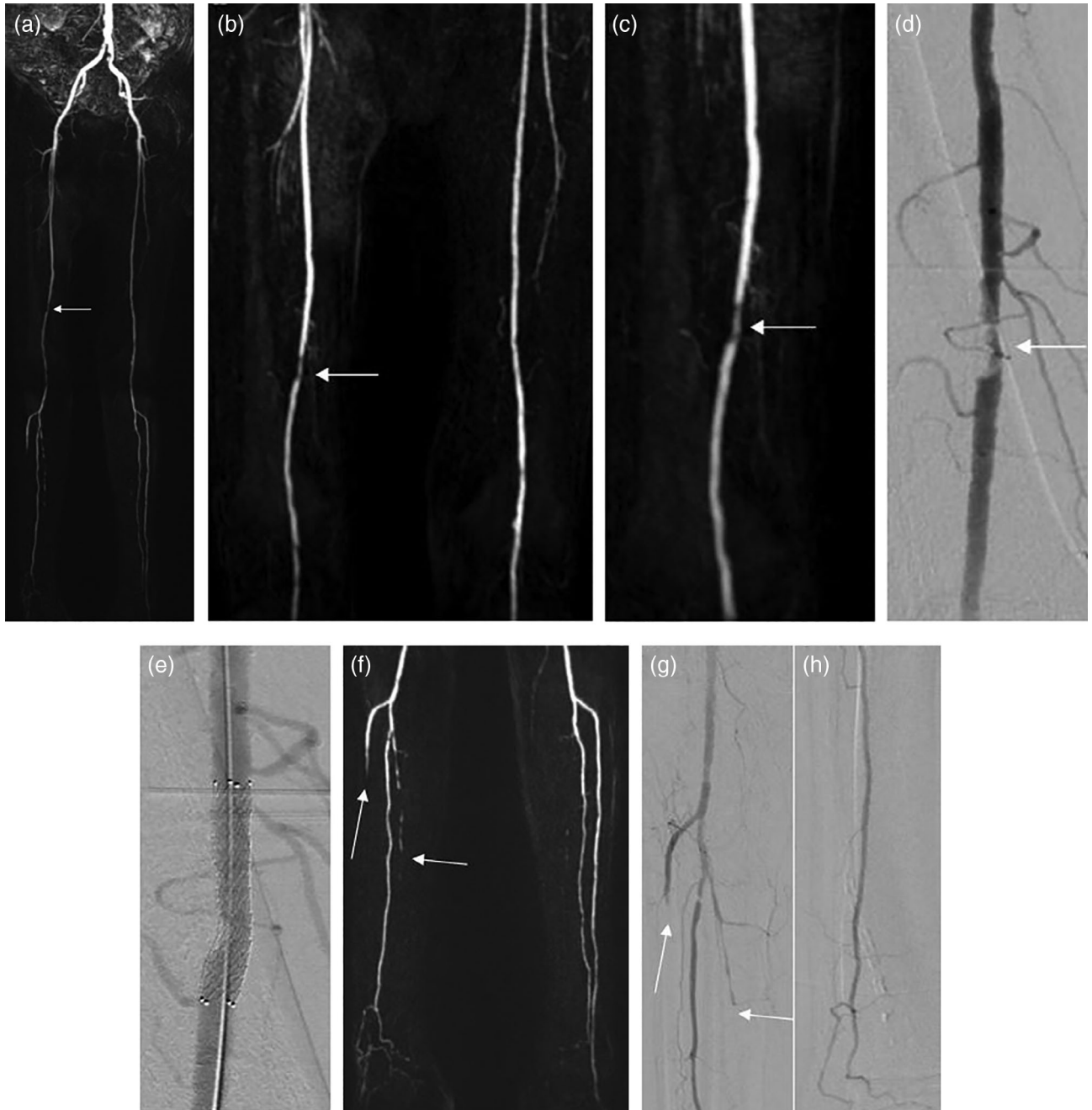


**FIGURE 3:** 81 year-old-male patient with symptoms of PAD and severely impaired kidney function. (a) MIP/MPR of subtracted TWIST-images of the lower extremities show multiple artery occlusion of the lower legs and a severe artery stenosis of the right superficial femoral artery (arrow). (b) Subtracted dynamic TWIST images and enlarged view (c) of the right femoral artery stenosis (arrow), DSA was performed afterwards and the severity of the stenosis was confirmed (arrow) (d). Stent-PTA was done for treatment (e). (f) Subtracted dynamic TWIST-images of both lower legs reveal proximal occlusion of the right anterior (vertical arrow) and posterior (horizontal arrow) tibial artery, which was confirmed in DSA afterwards (g,h).

**TABLE 4. Comparison of TWIST-MRA With DSA for the Detection of Significant Artery Stenosis**

Reader and Statistic	Overall Performance ( <i>n</i> = 256)	Pelvis ( <i>n</i> = 61)	Thigh ( <i>n</i> = 85)	Lower Legs ( <i>n</i> = 110)
Reader 1				
Sensitivity (%)	95.1 (86.3–99)	100 (71.5–100)	95.5 (77.2–99.9)	92.9 (81.7–99.9)
Specificity (%)	98 (94.8–99.4)	98 (89.4–99.9)	96.8 (89–99.6)	98.8 (93.4–99.9)
Positive predictive value (%)	93.6 (84.6–97.5)	91.7 (61.2–98.7)	91.3 (72.8–97.6)	96.4 (79.4–99.5)
Negative predictive value (%)	98.5 (95.5–99.5)	100 (N.A.)	98.4 (90–99.8)	98.8 (92.2–99.8)
Accuracy (%)	97.3 (94.5–98.9)	98.4 (91.2–99.9)	96.5 (90–99.3)	98.2 (93.6–99.8)
Reader 2				
Sensitivity (%)	96.8 (88.8–99.6)	100 (71.5–100)	95.7 (78.05–99.9)	96.4 (81.7–99.9)
Specificity (%)	98.5 (95.6–99.7)	100 (92.9–100)	98.4 (91.3–99.9)	98.8 (93.4–99.9)
Positive predictive value (%)	95.2 (86.7–98.4)	100 (N.A.)	95.7 (75.9–99.4)	96.4 (79.4–99.5)
Negative predictive value (%)	99 (96.1–99.7)	100 (N.A.)	98.4 (90–99.8)	98.8 (92.2–99.8)
Accuracy (%)	98.1 (95.5–99.4)	100 (94.1–100)	97.7 (91.8–99.7)	98.2 (93.6–99.8)
Reader 3				
Sensitivity (%)	96.7 (88.7–99.7)	100 (71.5–100)	95.5 (77.2–99.9)	96.4 (81.7–99.9)
Specificity (%)	98.5 (95.6–99.7)	100 (92.9–100)	98.3 (91.1–99.9)	97.6 (91.5–99.7)
Positive predictive value (%)	95.2 (86.5–98.4)	100 (N.A.)	93.6 (84.6–97.5)	93.1 (77.4–98.2)
Negative predictive value (%)	98.9 (96.1–99.7)	100 (N.A.)	98.3 (89.7–99.8)	98.8 (92.1–99.8)
Accuracy (%)	98.1 (95.5–99.4)	100 (94.1–100)	97.6 (91.5–99.7)	97.3 (92.2–99.4)
DSA (stenoses)	<i>n</i> = 62	<i>n</i> = 11	<i>n</i> = 23	<i>n</i> = 28

Data in parentheses are 95%-confidence intervals, *n* = number of correlated artery segments; N.A. = Not Applicable.

### Inter-Reader Agreement

Excellent to almost perfect agreement among readers was achieved both for detection of significant artery stenosis and artery occlusion with ICC values >0.90 in every anatomic vessel region.

Overall comparison showed excellent correlation with ICC values of 0.95 for significant artery stenosis and 0.98 for artery occlusion. Moreover, ICC values were calculated for every anatomic station (pelvic, thigh, and lower leg station) yielding comparable values (ICC 0.98, 0.96, and 0.91 for significant artery stenosis and ICC 1.0, 1.0, and 0.98 for artery occlusion).

### Venous Overlay

No notable venous overlay (grade 2) leading to a loss of diagnostic—accuracy was observed in any artery segment in any of the 40 patients.

Mild venous overlay (grade 1) was noted in a total of 7 of 40 patients (17.5%); 3 artery segments in the pelvic region, 5 artery segments in the thigh region, and 12 artery segments in the lower leg region.

In 33 out of 40 patients (82.5%), no venous overlay (grade 0) was observed.

Mean values and standard deviation for grading of venous overlay ranged from  $0.11 \pm 0.37$  in the pelvic region to  $0.28 \pm 0.45$  in the lower leg region (see Fig. 4).

**TABLE 5. Comparison of TWIST-MRA With DSA for the Detection of Artery Occlusions**

Reader and Statistic	Overall Performance ( <i>n</i> = 256)	Pelvis ( <i>n</i> = 61)	Thigh ( <i>n</i> = 85)	Lower Legs ( <i>n</i> = 110)
Reader 1				
Sensitivity (%)	100 (87.2–100)	100 (2.5–100)	100 (59.1–100)	100 (82.4–100)
Specificity (%)	99.1 (96.9–99.9)	100 (94.1–100)	100 (95.4–100)	97.8 (92.4–99.7)
Positive predictive value (%)	93.1 (77.3–98.2)	100 (N.A.)	100 (N.A.)	90.5 (70.7–97.4)
Negative predictive value (%)	100 (N.A.)	100 (N.A.)	100 (N.A.)	100 (N.A.)
Accuracy (%)	99.2 (97.2–99.9)	100 (94.1–100)	100 (95.8–100)	98.2 (93.6–99.8)
Reader 2				
Sensitivity (%)	100 (87.7–100)	100 (2.5–100)	100 (59.1–100)	100 (82.4–100)
Specificity (%)	99.5 (97.6–99.9)	100 (94.1–100)	100 (95.4–100)	98.9 (94.1–100)
Positive predictive value (%)	97.6 (80–99.5)	100 (N.A.)	100 (N.A.)	95 (73.1–99.3)
Negative predictive value (%)	100 (N.A.)	100 (N.A.)	100 (N.A.)	100 (N.A.)
Accuracy (%)	99.6 (97.8–99.9)	100 (94.1–100)	100 (95.8–100)	99.1 (95.1–100)
Reader 3				
Sensitivity (%)	100 (87.7–100)	100 (2.5–100)	100 (59.1–100)	100 (82.4–100)
Specificity (%)	99.5 (97.6–99.9)	100 (94.1–100)	100 (95.4–100)	97.8 (92.4–99.7)
Positive predictive value (%)	97.6 (80–99.5)	100 (N.A.)	100 (N.A.)	90.5 (70.7–97.4)
Negative predictive value (%)	100 (N.A.)	100 (N.A.)	100 (N.A.)	100 (N.A.)
Accuracy (%)	99.6 (97.8–99.9)	100 (94.1–100)	100 (95.8–100)	98.2 (93.6–99.8)
DSA (occlusion)	<i>n</i> = 27	<i>n</i> = 1	<i>n</i> = 7	<i>n</i> = 19

Data in parentheses are 95%-confidence intervals, *n* = number of artery segments/artery occlusions, N.A. = not applicable.

Intraclass correlation coefficients revealed a good overall correlation with ICC values of 0.81 (pelvic region 0.85; thigh region 0.84; and lower leg region 0.77).

ANOVA revealed no statistically significant differences between readers with regard to grading of venous overlay (overall grades  $P = 0.88$ ; pelvic region  $P = 0.97$ ; thigh region  $P = 0.92$ ; and lower leg region  $P = 0.87$ ).

### Image Quality

Analysis of overall image quality yielded good to excellent ratings for all readers ( $3.41 \pm 0.72$ ,  $3.33 \pm 0.65$ , and  $3.38 \pm 0.61$  for readers 1, 2, and 3 respectively). A nonsignificant ( $P = 0.18$ ) decrease in image quality from the pelvic to the lower leg arteries was noted, due to decreasing vessel size

as well as increasing occurrence of collateral artery vessels in PAD (pelvic region  $3.69 \pm 0.63/3.61 \pm 0.65/3.54 \pm 0.51$ ; thigh region  $3.44 \pm 0.73/3.31 \pm 0.70/3.38 \pm 0.62$ ; and lower leg region  $3.22 \pm 0.75/3.18 \pm 0.59/3.27 \pm 0.63$ ). There were no patients in which image quality was considered nondiagnostic (Fig. 5).

Intraclass correlation coefficients revealed a good overall correlation with ICC values of 0.75 between readers (pelvic region 0.77; thigh region 0.71; and lower leg region 0.71).

ANOVA revealed no statistically significant differences between readers (overall rating  $P = 0.47$ ; pelvic region  $P = 0.93$ ; thigh region  $P = 0.87$ ; and lower leg region  $P = 0.18$ ).



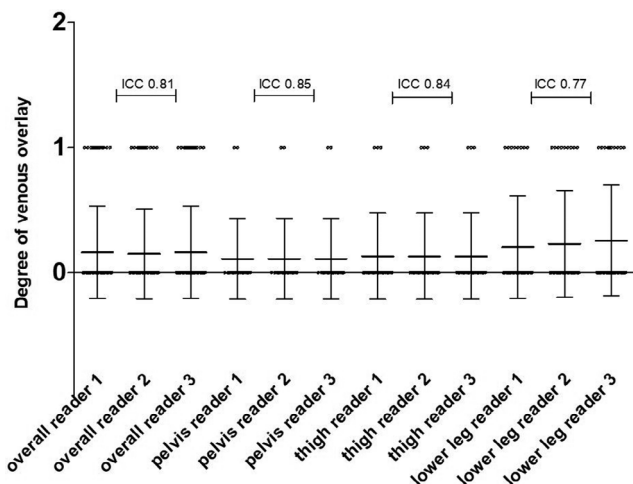


FIGURE 4: Scatter plots of venous overlay. Each spot represents a grade of each patient in a respective anatomic region. The vertical lines represent standard deviation with mean indicated as a thick horizontal line. ICC, intraclass correlation coefficient.

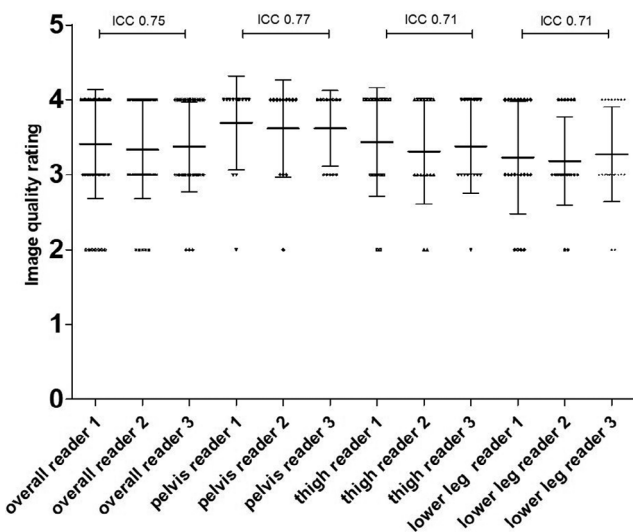


FIGURE 5: Scatter plots of image quality. Each spot represents a quality rating of each patient in a respective anatomic region. The vertical lines represent standard deviation with mean indicated as a thick horizontal line. ICC, intraclass correlation coefficient.

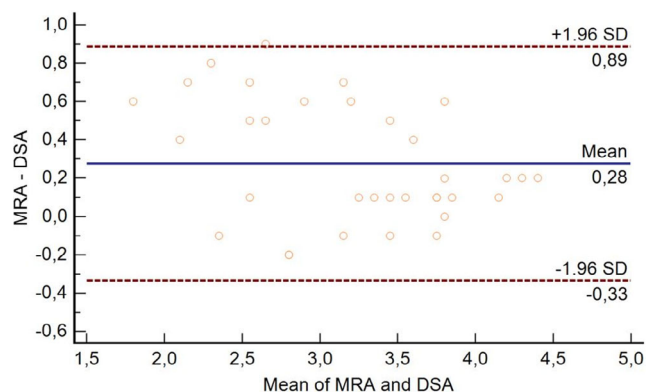


FIGURE 6: Bland-Altman comparison of average diameter stenosis (DS) in mm for iliac and femoropopliteal artery segments. Differences of means are plotted against the mean of MRA and DSA. SD = standard deviation.

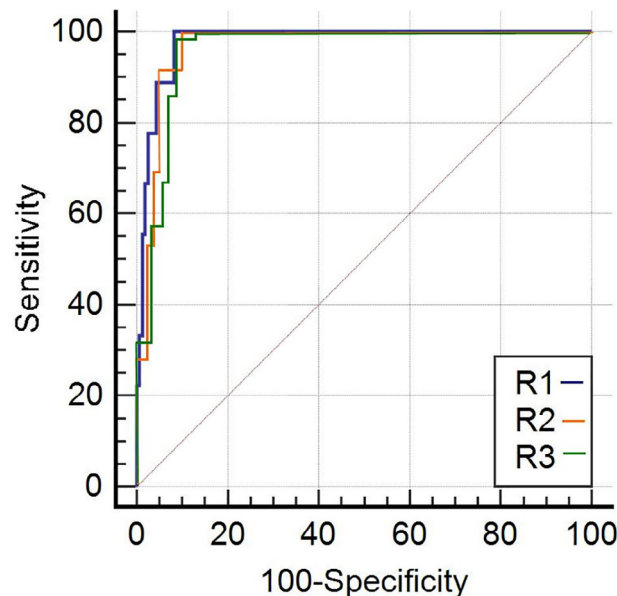


FIGURE 7: ROC curves of average DS values for >50% MRA stenosis R = reader (n = 3)

**DS Evaluation**

Average DS was evaluated for the correlated pelvic and thigh artery segments (n = 34). Due to small vessel caliber and acquired spatial resolution, infrapopliteal arteries could not be reliably evaluated with regard to DS quantification.

DS results were 3.08 ± 0.76 mm (mean ± SD) for DSA and 3.35 ± 0.64 mm (mean ± SD) for MRA, with only small differences of means (also see Fig. 6, Bland-Altman comparison).

ICC values showed good to excellent correlation between readers with 0.91 [95% CI: 0.57–0.97].

AUC of ROC curve analysis was 0.976 [95 %CI: 0.953–0.993] for reader 1; 0.965 [95% CI 0.935–0.984] for reader 2; and 0.96 [95%CI: 0.928–0.980] for reader 3 (see Fig. 7). No statistically significant differences between AUCs were noted by the DeLong comparison method (P = 0.66, P = 0.34, P = 0.21).

**Discussion**

The past 15 years has seen nephrogenic systemic fibrosis (NSF) and, more recently, gadolinium retention in the brain as potential problems associated with the administration of GBCAs. Although NSF now appears to be a problem of the past with no clear unconfounded cases reported over the past decade,<sup>28</sup> Gd retention is an ongoing concern with all currently FDA-approved GBCAs shown to be retained in human tissues to some extent (either as intact molecule or dissociated Gd bound to macromolecules).<sup>17,18</sup> Given concern over potential, as yet unidentified, health issues associated with long-term Gd retention in the brain, focus has turned toward the development of low GBCA dose MRI techniques.<sup>29–32</sup>

In patients suffering from PAD, dynamic MRA techniques including TWIST-MRA are particularly promising for the assessment of peripheral arteries as they provide functional information on inflow and outflow dynamics as well as information on vessel morphology.<sup>12,13,15</sup> However, achieving an adequate balance between temporal and spatial resolution while maintaining sufficiently high image quality across the entire peripheral vascular system from the pelvic to the lower leg region is still challenging and until recently, only feasible with the application of relatively large amounts of GBCA. In abdominal imaging, well-implemented dynamic MRI-sequences such as GRASP and compressed sensing techniques yield sufficient temporal and spatial resolutions in smaller anatomic areas (i.e., specific organs or lesions) such that lower GBCA doses of 0.05 mmol/kg bodyweight.<sup>33,34</sup>

A recent study by Kinner et al<sup>16</sup> evaluated the feasibility of using only dynamic flow images of the entire peripheral vascular system for the detection of peripheral artery stenosis and occlusion. Although they showed good correlation between MRA and DSA, the study lacked a dedicated diagnostic performance evaluation. Moreover, the signal-to-noise ratio in the study was low, which was ascribed in part to the 1.5 T magnetic field strength at which examinations were performed. Notably, however, relatively large amounts of GBCA were applied (15 mL of gadobutrol, 1.0 M, which corresponds to 30 mL of a standard 0.5 M GBCA formulation). As noted by the authors, this dose exceeded the standard dose used at that time (2012) for established, conventional MRA hybrid protocols, and is today two times higher than the currently recommended dose of gadobutrol.<sup>35</sup> It also goes against current recommendations to use the lowest diagnostic dose of GBCA possible.<sup>36</sup>

In our study, a much lower amount of GBCA (total of 9 mL, 0.5 M gadoteridol) was administered per patient, corresponding to 0.05–0.06 mmol/kg bodyweight. This is the lowest dose reported for a diagnostic contrast-enhanced MRA protocol of the entire lower extremities, with the exception of unenhanced MRA such as QISS-sequence protocols and pedal MRA protocols, limited only to the lower leg regions.<sup>8–10,37</sup> However, assessment of dynamic flow information does not only represent a “nice-to-have” feature, it more importantly also yields highly relevant information on vessel patency with regard to reversed perfusion or hemodynamic differences between adjacent peripheral arteries, thus providing a feature which no unenhanced MRA protocol can provide.

In this study, evaluation of diagnostic performance resulted in at least comparable sensitivity, specificity and overall diagnostic accuracy as previously published studies<sup>8,10,15,38</sup>. Sensitivity for detecting significant artery stenosis was 95.1%, exceeding the previously published values of 88%–91% in ce-MRA. One unenhanced MRA study showed a higher sensitivity in the detection of significant artery stenosis

(100%), but the corresponding specificity was diminished dramatically (76.5%), thus compromising overall diagnostic performance compared to ce-MRA protocols.<sup>10</sup>

In our study, overall specificity ranged from 97.6% to 98.5% for significant artery stenosis, surpassing values in the current literature which range from 87.4% to 96.8% in both ce-MRA and unenhanced MRA protocols.<sup>15,39,40</sup>

These previously published studies did not report the diagnostic performance for the detection of peripheral artery occlusion which in our study, was detected with near perfect sensitivity and specificity.

Overall diagnostic accuracy for the detection of artery stenosis in previously published literature has not exceeded 95%.<sup>8,10,15,38</sup> Our results, in contrast, showed values ranging from 96.5% to 100%.

A highly likely explanation for these apparently improved results lies in the dynamic image analysis available to assist grading the severity of stenosis, not only by vessel diameter but also by side-by-side comparison of inflow and outflow dynamics. This appears to have been especially helpful for the very small vessel diameters of the lower legs, where it is almost impossible to reliably measure the degree of stenosis by reduction in vessel width or caliber. Detection of severely impeded inflow and outflow, particularly with the help of contra-lateral flow comparisons, was considered to be straight forward by both readers, highly improving diagnostic confidence in the detection of significant stenosis in the lower legs and contributing to the high diagnostic accuracy reported in our results. Moreover, DSA also relies on the very same approach, combining morphological and dynamic impressions, to reach a diagnosis.

Comparison of diagnostic performance across readers revealed excellent to perfect correlation throughout, even though the readers had different levels of experience in assessing MR images. This observation implies that the MRA technique is reliable, accurate, and comparatively easy to evaluate even by junior readers with relatively low levels of radiological practice and experience.

Image quality analysis revealed good to excellent results in all patients and across both readers, with no segments deemed nondiagnostic. Similar findings were reported for evaluation of venous overlay, with none to only slight venous overlay noted in some segments that did not impair diagnostic confidence. In fact, significant venous overlay rating even in patients with strong vessel collateralization did not occur due to the availability of early to late dynamic contrast filling of each vessel in all anatomic areas, thus always providing full presentation of even small arteries before the appearance of contrast-enhanced veins in the same area.

These findings highlight a clear advantage over other MRA techniques, where both lack of image quality and—particularly in unenhanced MRA protocols—venous overlay in lower leg regions negatively affected results in diagnostic performance.<sup>10,39</sup>

Additionally, by only evaluating subtracted, dynamic MIP images of 4D MRA, the overall workload for image analysis was reduced, thus saving time in diagnosing PAD. Analysis of all original source images from the full 4D dynamic MRA protocol would have been much more time-consuming although this was not evaluated formally in this study.

## Limitations

First, retrospective studies are, by design and definition, prone to bias, thus our results need to be confirmed in larger, prospective trials. Furthermore, in our study, only a relatively small number of vessel segments could be correlated with DSA and subsequently evaluated for diagnostic performance. This was mainly because of the limited necessity to perform interventional DSA, which can be ascribed to the adequate image quality of our TWIST-MRA protocol, which in turn made pure diagnostic DSA obsolete.

Second, our MRA protocol demands a relatively large number of acquired images per patient. Consequently, fast dataset reconstruction is a challenging demand on computer hardware. However, improvements in computer hardware are common and still ongoing, therefore providing fast reconstruction options at almost every work station in modern radiology.

Finally, further studies are needed to evaluate the time savings achieved by performing diagnoses from MIPs rather than from original source images.

## Conclusion

Our study demonstrates the clinical feasibility and high diagnostic accuracy of a dynamic MRA protocol for the depiction of the entire runoff vasculature using a lower total gadolinium dose, providing dynamic flow information in every artery segment. Moreover, this was achieved by reviewing a limited number of MIP images, and the original source data in case of questionable pathological findings, thereby potentially reducing analysis time.

## Acknowledgments

Siemens Healthineers provided the MR sequence for this study, but had no role in study design, data collection and analysis, decision to publish, or preparation of the manuscript. The authors received no specific funding for this original research. Open Access funding enabled and organized by Projekt DEAL.

## REFERENCES

- Escobar C, Blanes I, Ruiz A, et al. Prevalence and clinical profile and management of peripheral arterial disease in elderly patients with diabetes. *Eur J Intern Med* 2011;22(3):275-281.
- Leng GC, Lee AJ, Fowkes FG, et al. Incidence, natural history and cardiovascular events in symptomatic and asymptomatic peripheral arterial disease in the general population. *Int J Epidemiol* 1996;25(6):1172-1181.
- Ghibes P, Hefferman G, Nikolaou K, et al. Quantitative evaluation of peripheral arterial blood flow using Peri-interventional fluoroscopic parameters: An in vivo study evaluating feasibility and clinical utility. *Biomed Res Int* 2020;2020(9526790):1-8.
- Hay JW, Lawler E, Yucel K, et al. Cost impact of diagnostic imaging for lower extremity peripheral vascular occlusive disease. *Value Health* 2009;12(2):262-266.
- Bui BT, Miller S, Mildenerger P, Sam A, Sheng R. Comparison of contrast-enhanced MR angiography to intraarterial digital subtraction angiography for evaluation of peripheral arterial occlusive disease: Results of a phase III multicenter trial. *J Magn Reson Imaging* 2010;31(6):1402-1410.
- Vogt FM, Zenge MO, Ladd ME, et al. Peripheral vascular disease: Comparison of continuous MR angiography and conventional MR angiography—pilot study. *Radiology* 2007;243(1):229-238.
- Scherthaner R, Stadler A, Lomoschitz F, et al. Multidetector CT angiography in the assessment of peripheral arterial occlusive disease: Accuracy in detecting the severity, number, and length of stenoses. *Eur Radiol* 2008;18(4):665-671.
- Hodnett PA, Ward EV, Davarpanah AH, et al. Peripheral arterial disease in a symptomatic diabetic population: Prospective comparison of rapid unenhanced MR angiography (MRA) with contrast-enhanced MRA. *AJR Am J Roentgenol* 2011;197(6):1466-1473.
- Klasen J, Blondin D, Schmitt P, et al. Nonenhanced ECG-gated quiescent-interval single-shot MRA (QISS-MRA) of the lower extremities: Comparison with contrast-enhanced MRA. *Clin Radiol* 2012;67(5):441-446.
- Hansmann J, Morelli JN, Michaely HJ, et al. Nonenhanced ECG-gated quiescent-interval single shot MRA: Image quality and stenosis assessment at 3 tesla compared with contrast-enhanced MRA and digital subtraction angiography. *J Magn Reson Imaging* 2014;39(6):1486-1493.
- Versluis B, Nelemans PJ, Wildberger JE, Schurink GW, Leiner T, Backes WH. Magnetic resonance imaging-derived arterial peak flow in peripheral arterial disease: Towards a standardized measurement. *Eur J Vasc Endovasc Surg* 2014;48(2):185-192.
- Meissner OA, Rieger J, Weber C, et al. Critical limb ischemia: Hybrid MR angiography compared with DSA. *Radiology* 2005;235(1):308-318.
- Berg F, Bangard C, Bovenschulte H, et al. Hybrid contrast-enhanced MR angiography of pelvic and lower extremity vasculature at 3.0 T: Initial experience. *Eur J Radiol* 2009;70(1):170-176.
- Wang CC, Liang HL, Hsiao CC, et al. Single-dose time-resolved contrast enhanced hybrid MR angiography in diagnosis of peripheral arterial disease: Compared with digital subtraction angiography. *J Magn Reson Imaging* 2010;32(4):935-942.
- Attenberger UI, Haneder S, Morelli JN, Diehl SJ, Schoenberg SO, Michaely HJ. Peripheral arterial occlusive disease: Evaluation of a high spatial and temporal resolution 3-T MR protocol with a low total dose of gadolinium versus conventional angiography. *Radiology* 2010;257(3):879-887.
- Kinner S, Quick HH, Maderwald S, Hunold P, Barkhausen J, Vogt FM. Triple-TWIST MRA: High spatial and temporal resolution MR angiography of the entire peripheral vascular system using a time-resolved 4D MRA technique. *Eur Radiol* 2013;23(1):298-306.
- Murata N, Gonzalez-Cuyar LF, Murata K, et al. Macrocyclic and other non-group 1 gadolinium contrast agents deposit low levels of gadolinium in brain and bone tissue: Preliminary results from 9 patients with normal renal function. *Invest Radiol* 2016;51(7):447-453.
- Murata N, Murata K, Gonzalez-Cuyar LF, Maravilla KR. Gadolinium tissue deposition in brain and bone. *Magn Reson Imaging* 2016;34(10):1359-1365.

19. Bannas P, Finck-Wedel AK, Buhk JH, et al. Comparison of whole body MR angiography at 1.5 and 3 Tesla in patients with hereditary hyperlipidemia. *Acta Radiol* 2011;52(5):547-553.
20. Shen Y, Goerner FL, Snyder C, et al. T1 relaxivities of gadolinium-based magnetic resonance contrast agents in human whole blood at 1.5, 3, and 7 T. *Invest Radiol* 2015;50(5):330-338.
21. Attenberger UI, Michaely HJ, Wintersperger BJ, et al. Three-dimensional contrast-enhanced magnetic-resonance angiography of the renal arteries: Interindividual comparison of 0.2 mmol/kg gadobutrol at 1.5 T and 0.1 mmol/kg gadobenate dimeglumine at 3.0 T. *Eur Radiol* 2008;18(6):1260-1268.
22. Schieda N, Blachman JI, Costa AF, et al. Gadolinium-based contrast agents in kidney disease: A comprehensive review and clinical practice guideline issued by the Canadian Association of Radiologists. *Can J Kidney Health Dis* 2018;5:2054358118778573.
23. Song T, Laine AF, Chen Q, et al. Optimal k-space sampling for dynamic contrast-enhanced MRI with an application to MR renography. *Magn Reson Med* 2009;61(5):1242-1248.
24. Lim RP, Shapiro M, Wang EY, et al. 3D time-resolved MR angiography (MRA) of the carotid arteries with time-resolved imaging with stochastic trajectories: Comparison with 3D contrast-enhanced bolus-chase MRA and 3D time-of-flight MRA. *AJNR Am J Neuroradiol* 2008;29(10):1847-1854.
25. Roberson PK, Shema SJ, Mundfrom DJ, Holmes TM. Analysis of paired Likert data: How to evaluate change and preference questions. *Fam Med* 1995;27(10):671-675.
26. Stratton SJ. Likert Data. *Prehosp Disaster Med* 2018;33(2):117-118.
27. Baum RA, Rutter CM, Sunshine JH, et al. Multicenter trial to evaluate vascular magnetic resonance angiography of the lower extremity. American College of Radiology Rapid Technology Assessment Group. *JAMA* 1995;274(11):875-880.
28. Woolen SA, Shankar PR, Gagnier JJ, MacEachern MP, Singer L, Davenport MS. Risk of nephrogenic systemic fibrosis in patients with stage 4 or 5 chronic kidney disease receiving a group II gadolinium-based contrast agent: A systematic review and meta-analysis. *JAMA Intern Med* 2020;180(2):223-230.
29. Semelka RC, Ramalho J, Vakharia A, et al. Gadolinium deposition disease: Initial description of a disease that has been around for a while. *Magn Reson Imaging* 2016;34(10):1383-1390.
30. Semelka RC, Ramalho M, AlObaidy M, Ramalho J. Gadolinium in humans: A family of disorders. *AJR Am J Roentgenol* 2016;207(2):229-233.
31. McDonald RJ, McDonald JS, Kallmes DF, et al. Gadolinium deposition in human brain tissues after contrast-enhanced MR imaging in adult patients without intracranial abnormalities. *Radiology* 2017;285(2):546-554.
32. Sanyal S, Marckmann P, Scherer S, Abraham JL. Multiorgan gadolinium (Gd) deposition and fibrosis in a patient with nephrogenic systemic fibrosis—an autopsy-based review. *Nephrol Dial Transplant* 2011;26(11):3616-3626.
33. Attenberger UI, Liu J, Riffel P, et al. Quantitative perfusion analysis of the rectum using Golden-angle radial sparse parallel magnetic resonance imaging: Initial experience and comparison to time-resolved angiography with interleaved stochastic trajectories. *Invest Radiol* 2017;52(12):715-724.
34. Feng L, Grimm R, Block KT, et al. Golden-angle radial sparse parallel MRI: Combination of compressed sensing, parallel imaging, and golden-angle radial sampling for fast and flexible dynamic volumetric MRI. *Magn Reson Med* 2014;72(3):707-717.
35. Highlights of Prescribing Information; Gadovist (Gadobutrol, Bayer Health Care Pharmaceuticals, 1.0 M). Accessed on March 15, 2021. Available from: [https://www.accessdata.fda.gov/drugsatfda\\_docs/label/2011/201277s000lbl.pdf](https://www.accessdata.fda.gov/drugsatfda_docs/label/2011/201277s000lbl.pdf)
36. Thomsen HS, Morcos SK, Almen T, et al. Nephrogenic systemic fibrosis and gadolinium-based contrast media: Updated ESUR contrast medium safety committee guidelines. *Eur Radiol* 2013;23(2):307-318.
37. Ganguli S, Pedrosa I, Smith MP, Niendorf ER, Fredericks S, Rofsky NM. Low dose pedal magnetic resonance angiography at 3 tesla with time-resolved imaging of contrast kinetics: A feasibility study. *Invest Radiol* 2008;43(9):650-655.
38. Miyazaki M, Lee VS. Nonenhanced MR angiography. *Radiology* 2008;248(1):20-43.
39. Wagner M, Knobloch G, Gielen M, et al. Nonenhanced peripheral MR-angiography (MRA) at 3 tesla: Evaluation of quiescent-interval single-shot MRA in patients undergoing digital subtraction angiography. *Int J Cardiovasc Imaging* 2015;31(4):841-850.
40. Knobloch G, Gielen M, Lauff MT, et al. ECG-gated quiescent-interval single-shot MR angiography of the lower extremities: Initial experience at 3 T. *Clin Radiol* 2014;69(5):485-491.